Applied Catalysis B: Environmental 168-169 (2015) 385–395

Contents lists available at ScienceDirect

Applied Catalysis B: Environmental

journal homepage: www.elsevier.com/locate/apcatb

3-D flower like Ce–Zr–Cu mixed oxide systems in the CO preferential oxidation (CO-PROX): Effect of catalyst composition

Elisa Moretti[a,*], Loretta Storaro[a], Aldo Talon[a], Pietro Riello[a], Antonia Infantes Molina[b], Enrique Rodríguez-Castellón[b]

[a] Department of Molecular Sciences and Nanosystems, Ca'Foscari University of Venice, INSTM Venice Research Unit, Via Torino 155/B, 30172 Venice, Italy
[b] Departamento de Química Inorgánica, Cristalografía y Mineralogía, Facultad de Ciencias, Universidad de Málaga, Campus de Teatinos, E-29071 Málaga, Spain

ARTICLE INFO

Article history:
Received 10 October 2014
Received in revised form
12 December 2014
Accepted 21 December 2014
Available online 6 January 2015

Keywords:
Hydrogen
CO-PROX
Copper
Ceria
Ceria–zirconia
Flower-like morphology

ABSTRACT

Ce–Zr–Cu mixed oxide systems, with different contents of ZrO_2 and CuO, were prepared by slow co-precipitation method, leading to the formation of materials with a flower-like morphology. It was evaluated both the role of CuO loading (3–7 wt%), by maintaining constant the amount of ZrO_2 (7 wt%), and the role of ZrO_2 (2–10 wt%) with a fixed amount of CuO (7 wt%). The prepared catalysts were characterized by means of ICP-OES, SEM, N_2 physisorption, quantitative XRD, H_2-TPR, and XPS. Their catalytic performances in the preferential oxidation of CO in excess of H_2 (CO-PROX) were evaluated, in the 40–190 °C temperature range. Characterization and catalytic results showed that an optimum Zr/Ce molar ratio and CuO loading are required to attain the best catalytic performance over the studied nanostructured Ce/Zr/Cu oxide system. Characterization results revealed that, regardless of the sample composition, all of them presented similar flower-like morphology and textural properties. Instead, the catalyst composition determined the crystalline phases formed, their reducibility and surface distribution. The catalyst containing an intermediate ZrO_2 loading (7 wt%) and the highest studied CuO amount (7 wt%), FCZCu77, showed the higher fraction of undetectable CuO from XRD, that is the highest proportion of highly dispersed Cu species also observed from H_2-TPR. These characteristics justify how FCZCu77 catalyst exhibited a quite higher catalytic activity than the others samples.

1. Introduction

The preferential oxidation (CO-PROX) reaction is an efficient way to purify hydrogen produced by steam reforming of hydrocarbons and alcohols for application in proton exchange membrane fuel cell (PEMFC) for the removal of carbon monoxide, since the presence of CO impedes the H_2/O_2 reaction by the anode absorption of CO and the consequent poisoning. Optimum fuel cell efficiency requires complete removal of CO (<10 ppm) from the hydrogen-rich gas feed. The PROX reaction must fall down the concentration of CO in the gaseous mixtures rich in hydrogen avoiding the oxidation of H_2 (to produce water).

Current fundamental research for the removal of CO focuses on ceria-based catalysts such as monometallics Au [1–5], Pt [6–8], Pd [9,10], Ir [11], and copper oxide [11–20]. Although the binary CuO–CeO_2 system shows a good performance in the preferential CO oxidation process, several studies have been made with the purpose of improving their efficiency and stability by incorporation of additional components, such as activity promoters [21–25]. It is known that the high performances of CuO–CeO_2 based catalysts are attributable to the strong interaction between highly dispersed copper species and the ceria surface, which favours the formation of oxygen vacancies at the copper–ceria fringes, increasing the Cu reducibility [26–31]. The addition of Zr to ceria modifies the redox properties, the oxygen-storage capacity, and thermal resistance of cerium oxide [29,32–38]. The efficiency of these three-components catalysts, in comparison with CuO–CeO_2 and CuO–ZrO_2 binary systems, was found to be strongly dependent not only from the molar ratio among reagents but also from the morphological and structural characteristics of the materials that can influence both the interaction between the oxides and the dispersion of the active phase [39–44].

In previous papers [20,31], we have described the preparation of a nanostructured Ce/Zr/Cu oxide system with a 3-dimensional flower-like morphology and its CO-PROX catalytic activity by studying both the influence of the catalyst thermal treatment and

* Corresponding author. Tel.: +39 041236745; fax: +39 0412346735.
E-mail address: elisa.moretti@unive.it (E. Moretti).

http://dx.doi.org/10.1016/j.apcatb.2014.12.032
0926-3373/

Table 1
Elemental composition, textural and structural parameters of the studied catalysts.

Sample	[a] Zr/Ce(mol mol^{-1})	[a] CuO(mol g_{cat}^{-1}) × 10^{-4}	[b] SA_{BET}(m^2 g^{-1})	[b] V_p(cm^3 g^{-1})	[c] dp CuO(nm)	[d] H_2 uptake(mol g^{-1}) × 10^{-3}	[d] H_2/Cu(mol mol^{-1})
FCZCu27	0.03	8.92	23 ± 1	0.01	13	0.95	1.07
FCZCu37	0.05	8.77	25 ± 1	0.02	15	1.01	1.15
FCZCu57	0.08	8.79	26 ± 1	0.02	13	1.04	1.18
FCZCu77	0.11	8.82	28 ± 1	0.02	13	1.08	1.21
FCZCu107	0.17	8.81	29 ± 1	0.03	40	0.99	1.13
FCZCu73	0.11	3.76	28 ± 1	0.01	13	0.53	1.41
FCZCu75	0.11	6.28	28 ± 1	0.01	18	0.78	1.24

[a] Determined by ICP-OES.
[b] N_2 adsorption–desorption data.
[c] CuO Crystallite sized determined from XRD by the Warren–Averbach's equation, with an estimated error of 10%.
[d] H_2-TPR data.

the influence of the layered morphology of the nanostructures with regard to samples prepared by the traditional co-precipitation method. In this work, we report the preparation of 3-D flower-like morphology Ce–Zr–Cu mixed oxide systems presenting different composition: low copper (3–7 wt%) and very low zirconia loading (2–10 wt%); and their activity and selectivity in the preferential oxidation of CO in H_2-rich gas streams. The main goal of this work is investigating the role of Zr and Cu content on the structure and catalytic response of Ce/Zr/Cu mixed oxide catalysts in CO-PROX reaction.

2. Experimental

2.1. Reagents

All the materials used are Aldrich products and no further purification was carried out.

2.2. Preparation of CeZrCu based oxide systems

A family of Ce–Zr–Cu mixed oxides, with different ZrO_2 and CuO loadings were prepared. Thus, in a typical synthesis for a catalyst containing 7 wt% of ZrO_2 and 7 wt% of CuO, 0.30 M aqueous solution of K_2CO_3 was slowly added (0.4 mL min^{-1}) to an aqueous solution of $CuCl_2{\cdot}2H_2O$ (1.4 mmol), $CeCl_3{\cdot}7H_2O$ (8.1 mmol) and $ZrOCl_2{\cdot}8H_2O$ (0.9 mmol) under stirring, to reach a pH value of 8.2. The resulting suspension was allowed to settle for 20 h. The resultant solid was separated through centrifugation, washed with deionized water till the complete disappearance of chlorides ($AgNO_3$ test), dried overnight at 80 °C and calcined up to 650 °C for 5 h (3 °C min^{-1}).

The samples will be referred to as FCZCu*xy*, where: F = flower-like; C = cerium; Z = zirconium; Cu = copper; *xy* is the nominal composition (wt% amount) of ZrO_2(*x*) and CuO(*y*) and CeO_2 being the remaining to 100%. For example in FCZCu77 sample, CeO_2, ZrO_2 and the CuO contents are 86.0 wt%, 7.0 wt%, and 70 wt%, respectively. To evaluate the role of Zr, five samples were prepared: FCZCu27, FCZCu37, FCZCu57, FCZCu77, and FCZCu107. While to evaluate the role of Cu, three samples were synthesized: FCZCu37, FCZCu57, and FCZCu77.

The metal content was determined by ICP-OES elemental analysis and the corresponding values are included in Table 1. A very small amount of chlorine was detected in the XPS survey spectra.

2.3. Catalytic activity measurements

Catalytic activity tests were carried out in a laboratory flow apparatus with a fixed bed reactor operating at atmospheric pressure. The catalyst, with a defined particle size (0.050–0.110 mm), was introduced into a tubular Pyrex glass reactor (5 mm i.d.), placed in an aluminum heating block.

Before the catalytic experiments, the sample was heated in situ at 400 °C under flowing filtered atmospheric air for 1 h. The gas hourly space velocity (GHSV) was 22,000 h^{-1}. The feed consisted of 1.25% CO, 1.25% O_2, and 50% H_2 (vol%) balanced with He. Calibration of the GC was done with a gas mixture containing 1% CO, 1% CO_2, and 1% O_2 in He.

The effect of CO_2 and H_2O was examined by adding both CO_2 (15 vol%) and H_2O (10 vol%) to the reaction stream using a HPLC pump (Jasco). The GC calibration, when the gas feed was CO_2 rich, was done with 15 vol% CO_2 in He. The gas lines were heated at 120 °C, to avoid water condensation before the reactor inlet. An ice-cooled water condenser was used to trap the excess of water downstream of the reactor. A HP6890 GC gas chromatograph equipped with a thermal conductivity detector was used to analyze the outlet composition. A CP Carboplot P7 column was used, with helium as a carrier. The detection limit for CO was 10 ppm. The temperature was varied in the 40–190 °C range, and measurements were carried out till a steady state was achieved. Both methanation and reverse water–gas-shift reactions were found to be negligible in the experimental conditions. The carbon monoxide and oxygen conversions were calculated based on the CO (Eq. (1)) and O_2 (Eq. (2)) consumption, respectively:

$$\text{CO Conversion}\,(\%) = \frac{n_{CO}^{in} - n_{CO}^{out}}{n_{CO}^{in}} \times 100 \quad (1)$$

$$O_2\text{Conversion}\,(\%) = \frac{n_{O_2}^{in} - n_{O_2}^{out}}{n_{O_2}^{in}} \times 100 \quad (2)$$

The selectivity towards CO_2 was estimated from the oxygen mass balance as follows (Eq. (3)):

$$\text{Selectivity}(\%) = \frac{n_{CO}^{in} - n_{CO}^{out}}{2\left(n_{O_2}^{in} - n_{O_2}^{out}\right)} \times 100 \quad (3)$$

The excess oxygen factor (λ) is defined as (Eq. (4)):

$$\lambda = 2 \times \frac{n_{O_2}^{in}}{n_{CO}^{in}} \quad (4)$$

Catalytic tests were performed using a λ = 2, founded as optimal for CO-PROX reaction in previous works [30,31].

To determine the apparent activation energy, E_a, experiments in differential conditions were performed in the temperature range 50–100 °C, to obtain CO conversion values below 15%.

2.4. Characterization techniques

Inductively coupled plasma (ICP-OES) analyses were performed with a PerkinElmer Optima 3100 XL spectrometer.

Scanning electron microscopy (SEM) images were taken with a JEOL JSM-5600LV, operated at 20 kV and using secondary electrons to form the image. The sample was coated with a thin layer of gold.

Nitrogen adsorption–desorption measurements were performed at liquid nitrogen temperature (−196 °C) with an ASAP 2010

apparatus of Micromeritics. Before each measurement, the samples (0.1 g) were outgassed first at 130 °C for 12 h at 5×10^{-3} Torr and then at room temperature for 2 h at 0.75×10^{-6} Torr. The N_2 isotherms were used to determine the specific surface areas through the BET equation (SA_{BET}), and the specific pore volume (V_s) calculated at $P/P_0 = 0.98$.

X-ray powder diffraction patterns (XRPD) were obtained using a Philips X'Pert system with a Cu Kα radiation (λ = 1.54184 Å). The samples were disc shaped pressed powders and spectra were collected after calcination. The average dimension of the crystallites was determined by the Scherrer method for copper and Warren–Averbach's equation for CeO_2–ZrO_2 solid solutions (the estimated errors are 10% ca).

Hydrogen temperature-programmed reduction (H_2-TPR) experiments were carried out using an AUTOCHEM 2910 instrument from Micromeritics. Approximately 0.1 g of freshly calcined catalyst were placed on top of some wool glass in a quartz reactor. In order to remove contaminants, the powder was pre-treated in helium (20 mL min^{-1}) to 350 °C for 1 h. After cooling to ambient temperature, the TPR experiments were carried out in 10 vol% H_2/Ar (30 mL min^{-1}) increasing the temperature from 40 °C to 800 °C (10 °C min^{-1}), by a temperature programmable controller. A Dewar flask containing a liquid nitrogen/ethanol slurry was used as cryogenic trap to prevent water to contact the detector.

X-Ray photoelectron spectra (XPS) were collected using a Physical Electronics PHI 5700 spectrometer with non monochromatic Mg Kα radiation (300 W, 15 kV, 1253.6 eV) for the analysis of the core level signals of C 1s, O 1s, Zr 3d, Ce 3d and Cu 2p and with a multichannel detector. Spectra of powdered samples were recorded with the constant pass energy values at 29.35 eV, using a 720 μm diameter analysis area. During data processing of the XPS spectra, binding energy values were referenced to the C 1s peak (284.8 eV) from the adventitious contamination layer. The PHI ACCESS ESCA-V6.0 F software package was used for acquisition and data analysis. A Shirley-type background was subtracted from the signals. Recorded spectra were always fitted using Gauss–Lorentz curves, in order to determine the binding energy of the different element core levels more accurately. The error in BE was estimated to be ca 0.1 eV. A short acquisition time of 10 min was used to examine C 1s, Cu 2p and Cu LMM XPS regions in order to avoid, as much as possible,

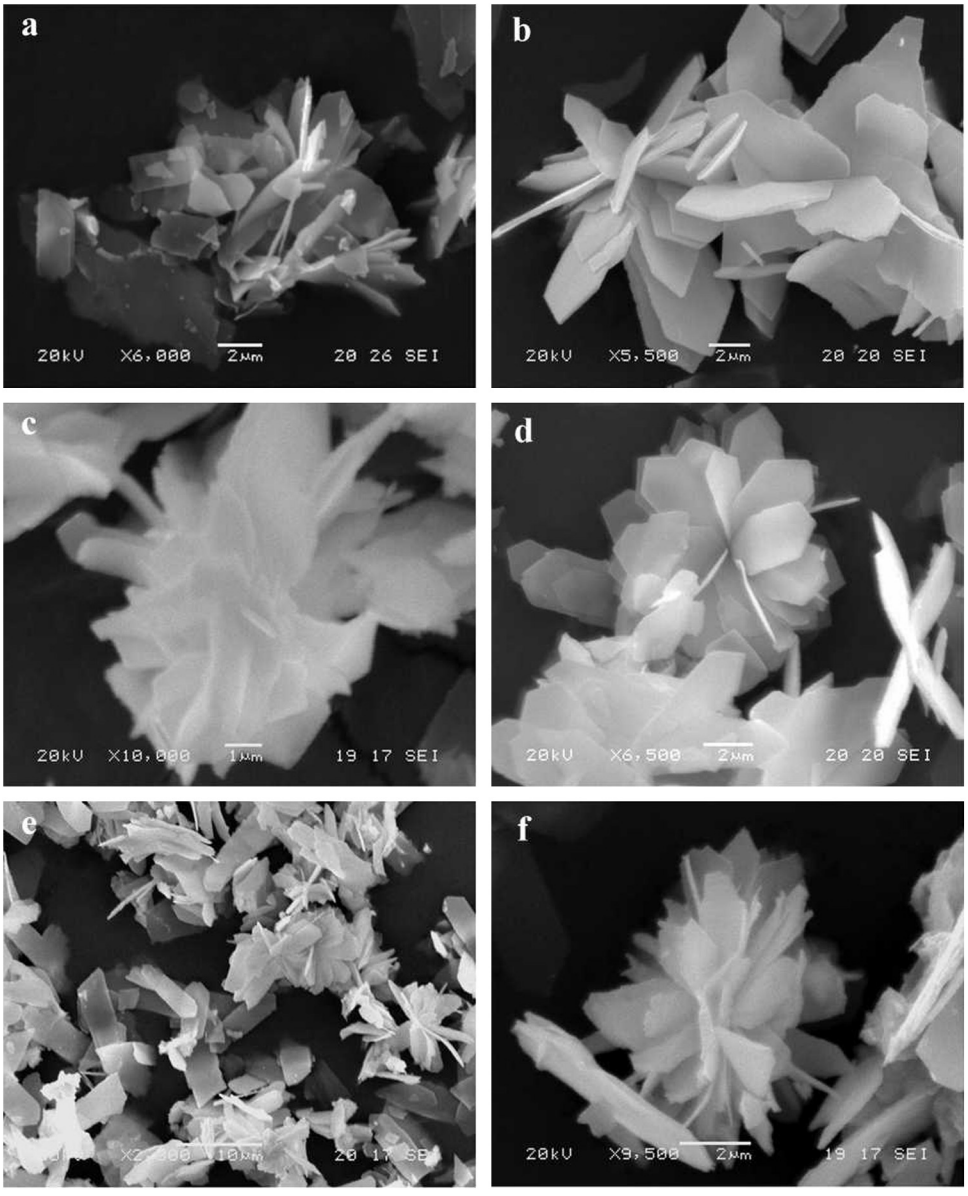

Fig. 1. SEM micrographs of: (a) FCZCu27; (b) FCZCu37; (c) FCZCu57; (d) FCZCu77; (e) FCZCu107; and (f) FCZCu73.

photoreduction of Cu^{2+} species. Nevertheless, a Cu^{2+} reduction in high vacuum during the analysis cannot be excluded [45].

3. Results and discussion

3.1. Elemental analysis (ICP-OES)

Ce, Zr, and Cu content in the prepared catalysts were determined from ICP-OES. The resulting values in terms of Zr/Ce molar ratio and CuO content (mol g_{cat}^{-1}) are included in Table 1. As expected, the Zr/Ce ratio increased with the amount of ZrO_2 added in the synthesis media, meanwhile CuO content was very closed for all these samples, synthesized with a nominal CuO composition of 7 wt%. On the other hand, samples containing different CuO nominal values also showed an increased CuO content value by raising the nominal loading. These data point to the feasibility of the proposed method to prepare 3-D flower like Ce–Zr–Cu mixed oxide systems presenting different compositions.

3.2. Scanning electron microscopy (SEM)

The 3D nanostructures with a flower like morphology have been previously described in the Cu/Ce/Zr three components oxide system prepared by a simple room temperature very slow addition of a K_2CO_3 solution to an aqueous solution of the precursors salts, followed by a long crystallization step at RT, in the absence of organic additives, generally used to hydrothermally prepared materials with this kind of nano-architectures [20,31]. It was suggested that the 3D architectures must be generated by some type of self-assembly occurring while the crystal growth is progressing. It is known that rare earths can crystallize from solutions containing carbonate ions, as orthorhombic or hexagonal phases of hydroxycarbonates, constituted by alternate stacks of cations and carbonate anions that sometimes are organized with shuttle-like, butterfly-like, or flower-like homocentric morphologies.

SEM micrographs showed that the morphology of $CuO–ZrO_2–CeO_2$ systems is flower-like independently from the Zr/Ce atomic ratio used. The structures are made up of long (>10 nm) and thin (about 200 nm) petals with quite homogeneous size and shape (Fig. 1a–f).

3.3. N_2 adsorption–desorption isotherms at −196 °C

The textural properties of the prepared catalysts in terms of specific surface area (SA_{BET}) and pore volume were calculated from their corresponding N_2 adsorption–desorption isotherms. The obtained values are included in Table 1. For samples containing different ZrO_2 content, it is observed that the specific surface area and pore volume slightly increased with ZrO_2 content. While the textural properties of the samples with different CuO loadings remained unchanged. In any case, the textural properties are very close in all cases, indicating that they are not affected by changes in the sample composition. It should be taken into account that the loading difference between the sample containing the lowest amount of ZrO_2 + CuO (FCZCu27) and that with the highest amount (FCZCu107) is only 8 wt%.

3.4. X-Ray powder diffraction (XRD)

The XRD patterns of the catalysts are presented in Fig. 2. All the diffraction patterns show the characteristic reflections of CeO_2 (fluorite structure JCPDS No. 43-1002) and the presence of very small peaks at $2\theta = 35.5°$ and 38.5°, due to small clusters of copper oxide as tenorite (No. 01-089-2529 in JCPDS database), with particle sizes of 13.0–40.0 nm, calculated by Scherrer analysis. Moreover, except the samples with lower content of zirconium oxide (2 and 3 wt%), all diffractograms show the presence of a shoulder near the main

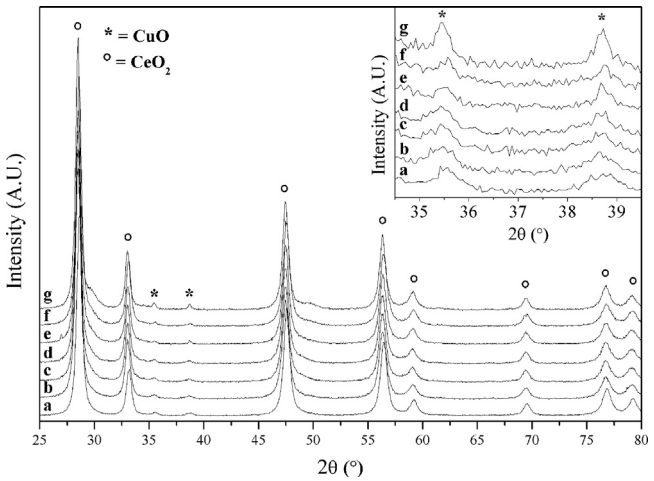

Fig. 2. XRPD patterns of FCZCuxy samples and magnification of the region 35–40° of 2I in the inset.

peaks of CeO_2 that can be assigned to a solid solution of $CeO_2–ZrO_2$ very rich in ZrO_2.

As described in detail in a previous work [20], the size of the cubic cerium oxide crystallites were calculated by the Warren–Averbach analysis of the diffraction lines and were found to be very similar, 14 nm. Since the broadening of two peaks can be compared with different orders of hkl, we used the Warren–Averbach (WA) analysis to evaluate the crystallite size taking into account the contributions of microstrain to the X-ray diffraction (XRD) profile broadening. A careful Rietveld study of the diffraction patterns allowed us to obtain quantitative information on the composition and on the distribution of the different oxides. The Vegard law $Vc = 158.84(\pm0.16) - 24.12(\pm0.26)x$ relates the composition of the solid solutions $Zr_xCe_{(1-x)}O_2$ to the unit cell volume Vc (the details of this analysis are described in Appendix A of a previous work [20]). The obtained values are included in Table 2.

Rietveld analysis showed the presence of three main species: a cubic phase of CeO_2 partially substituted by Zr, $Zr_xCe_{(1-x)}O_2$ where x ranges from 0.011 to 0.029; a tetragonal $Zr_xCe_{(1-x)}O_2$ phase with a greater Zr incorporation than before (x ranges from 0.49 to 0.80) and only noticeable for ZrO_2 loadings higher than 5 wt%; and CuO monoclinic phase, present in all the prepared samples.

Quantitative data indicate that by increasing ZrO_2 loading during synthesis, the incorporation to the cubic CeO_2 phase raises from FCZCu27 (0.011) to FCZCu37 (0.025), the addition of more Zr species to the synthesis media does not provoke further incorporation of Zr to this structure as, seen for FCZCu57, FCZCu77, and FCZCu107 samples, where $x = 0.022$, 0.020, and 0.027, respectively. However, the formation of the tetragonal $Zr_xCe_{(1-x)}O_2$ phase strongly depends on the Zr amount incorporated. Thus, the samples with low ZrO_2

Table 2
Quantitative Rietveld analysis of FCZCuxy samples.

Sample	[a] $Zr_xCe_{(1-x)}O_2$ (x) (wt%)	[b] $Zr_xCe_{(1-x)}O_2$ (x) (wt%)	[c] CuO (wt%)
FCZCu27	(0.011) 96.0 ± 1.0	–	4.0 ± 0.3
FCZCu37	(0.025) 94.5 ± 1.0	–	5.5 ± 0.8
FCZCu57	(0.022) 89.6 ± 1.0	(0.49) 5.1 ± 1.0	5.3 ± 0.6
FCZCu77	(0.020) 90.7 ± 1.0	(0.70) 6.9 ± 1.0	2.4 ± 0.7
FCZCu107	(0.027) 86.4 ± 1.0	(0.80) 7.9 ± 1.0	5.7 ± 0.5
FCZCu73	(0.022) 94.2 ± 1.0	(0.80) 4.2 ± 1.0	1.6 ± 0.6
FCZCu75	(0.029) 89.7 ± 1.0	(0.51) 7.5 ± 1.0	2.8 ± 0.4

[a] Cubic $Zr_xCe_{(1-x)}O_2$ phase.
[b] Tetragonal $Zr_xCe_{(1-x)}O_2$ phase.
[c] Monoclinic CuO phase.

loading (2–3 wt%) do not show the presence of this phase and it is when the ZrO_2 loading reaches 5 wt% that this phase becomes noticeable in XRD patterns and therefore in Rietveld quantitative analysis. It is observed a correlation between the Zr/Ce ratios obtained from ICP-OES analysis and the amount of zirconium incorporated to the tetragonal phase and the amount of such a phase formed. On the other hand, changes in CuO content do not affect the Zr incorporation into the cubic phase, but to the incorporation of Zr into the tetragonal one. Thus, it is observed a sharp decrease in Zr incorporation (x) from the sample with 3 wt% of CuO (0.8) to that with a 5 wt% (0.51). Later it increases for the sample with 7 wt% (0.7). No correlation is observed, by considering CuO contents calculated from Rietveld. The amount of tetragonal phase depends on ZrO_2 content: the higher this content, the higher the formation of such a phase. Finally, data included in Table 2 also show that the loaded amount of CuO, for all the samples, was larger than the calculated fraction by Rietveld analysis, which suggests that copper could be present as undetectable very small nanoparticles, substitutional copper ions in the ceria lattice or, owing to the small size of the Cu^{2+} ion, as interstitial punctual defects. This finding confirms the results obtained in the previous cited paper [20].

By comparing all the samples with the same nominal CuO composition (7 wt%), the sample FCZCu77 has the highest fraction of undetectable CuO (4.6 wt%).

3.5. Hydrogen temperature-programmed reduction (H_2-TPR)

The H_2-temperature programmed reduction (H_2-TPR) profiles of the fresh calcined samples with different ZrO_2 content are displayed in Fig. 3, while the H_2 consumption values and the exceeding the stoichiometric ones (H_2/Cu molar ratio) for all the samples are reported in Table 1. All the samples showed quite complex H_2-TPR profiles, reflecting the heterogeneity of the existing copper species.

The reduction of copper oxide supported on CeO_2 [27,46,47] and CeO_2–ZrO_2 [39,41] was observed to start above 100 °C, while pure CuO is reduced above 250 °C. Promotion of the copper species reduction by ceria was reported by several authors [46–49] and the reducibility was found to increase with the decreasing size of CuO particles [27,50]. As known pure zirconia cannot be reduced in hydrogen below 930 °C and ceria does not show any reduction peak below 500 °C [39]. Avgouropoulos et al. [27,46,51], studying the reduction of CuO on ceria attributed the peak at about 170 °C to the reduction of highly dispersed CuO strongly interacting with the ceria surface and two peaks at 220 °C and 255 °C to the reduction of larger copper oxide particles weakly interacting with ceria. Dong et al. [41] observed a broad reduction peak with a shoulder at low temperature, attributed to the reduction of highly dispersed copper oxide species interacting with ceria, and a peak at higher temperature attributable to the reduction of bulk-like CuO. Ratnasamy et al. [39] studying CuO on different supports showed that the copper oxide reducibility increases in the order $CuO–ZrO_2 < CuO–CeO_2–ZrO_2 < CuO–CeO_2$. Luo et al. [48] observed on $CuO–CeO_2$ catalysts a two-step reduction profile indicating the existence of two CuO species. The low temperature peak was associated to small CuO particles finely dispersed and interacting with ceria, while the higher temperature one was assigned to the reduction of larger CuO particles. Zou et al. [52] suggested, for the more complex H_2-TPR profiles, the contribution of both copper clusters and isolated Cu^{2+} ions.

As reported in previous works, the H_2-TPR complex profile showed by Ce–Zr–Cu mixed oxide systems with a flower-like morphology, is composed by several overlapped peaks, that can be mainly attributed, at low temperatures (<200 °C), to the reduction of oxidized copper species with different structural/morphological properties [20,31]. In some extent, H_2 uptake can be also ascribed to some concomitant phenomena such as the partial reduction of

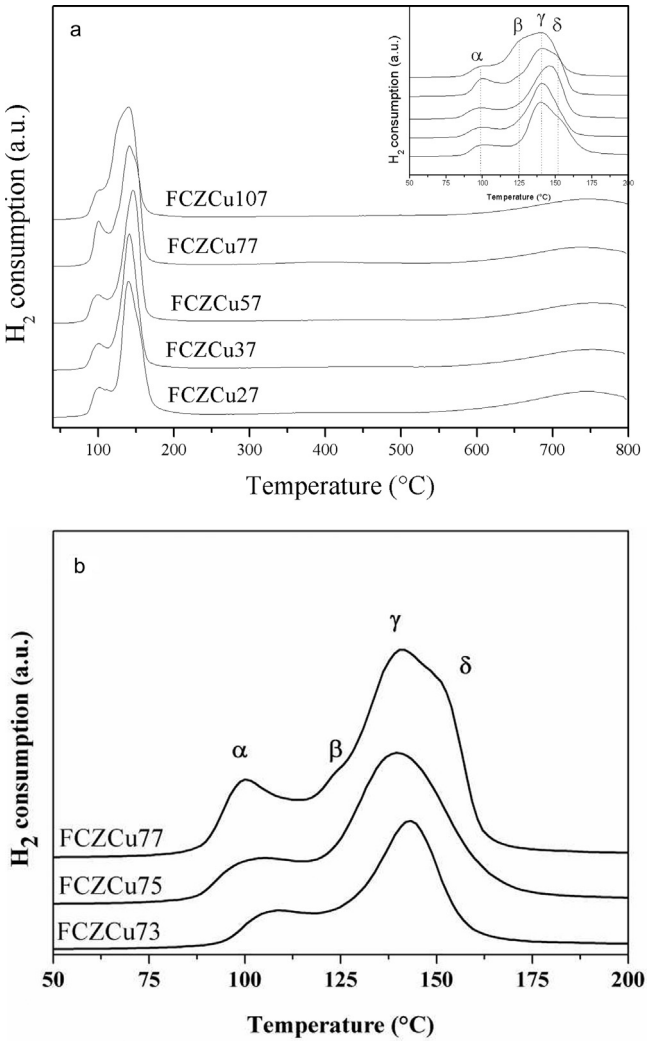

Fig. 3. H_2-TPR profiles of (a): catalysts with different Zr loading and magnification (in the inset) of the region 50–200 °C; (b) catalysts with different Cu loading.

ceria surface and to spillover of hydrogen on the support surface. Therefore the assignment of each reduction process is not easy. According to literature data and our previous results, TPR profiles (Fig. 3a and b) can be resolved in four overlapped peaks. The first peak (α) was generally attributed to the reduction of highly dispersed copper oxide species, strongly interacting with ceria; the second peak (β) to small two- and three-dimensional clusters of copper oxide weakly associated with the ceria; the third peak (γ) often quite intense, to the presence of CuO both in solid solution or as interstitial/substitutional defect in the ceria lattice; and finally, the peak named δ was ascribed to the reduction of Cu^{2+} ions of the bulk-type CuO particles in crystalline phase as observed in XRD patterns. Moreover, it is also observed a large broad peak centred at about 750 °C due to the partial reduction of Ce^{4+}–Ce^{3+} of medium–large ceria crystallites [17,53,54].

Comparing the TPR profiles of the samples containing the same amount of CuO (7 wt%) and different amount of zirconia (Fig. 3a) in the region of copper species reduction (<200 °C), it can be observed that α peak is more pronounced when the catalyst contains an intermediate amount of zirconia (FCZCu77) and becomes less intense both at lower and at higher Zr/Ce molar ratio. The formation of highly dispersed Cu species, responsible for α peak, could be ascribed to the known disorder and defects induced by the presence of zirconia in relatively small quantities in the ceria lattice. In fact, this sample, FCZCu77, possesses the highest amount of

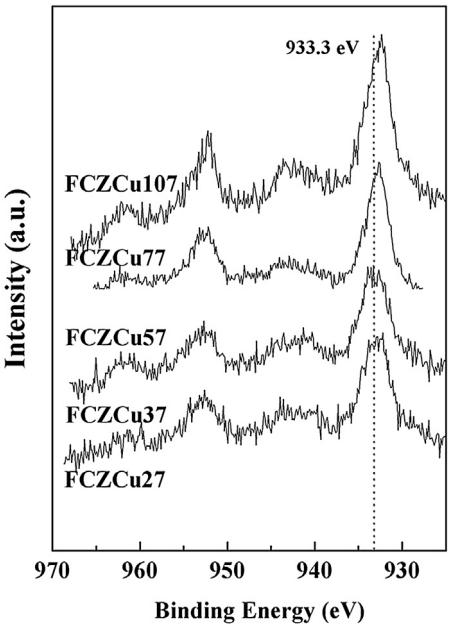

Fig. 4. Cu 2p core level spectra of the fresh catalysts containing a fixed copper content and different Zr/Ce molar ratio.

undetectable CuO from XRD, that is, the highest proportion of highly dispersed Cu species.

A magnification of the H_2-temperature programmed reduction (H_2-TPR) profiles of the samples containing the same nominal amount of zirconium Zr/Ce (0.11) and a different amount of copper in the region of copper species reduction is displayed in Fig. 3b. From this figure it is observed a slight shift of the easily reducible Cu-species broad peak to lower temperatures by increasing CuO loading. So the addition of a limited loading of copper seems to increase the amount of highly dispersed copper oxide species. These data suggests that a relatively high amount of copper appears to be required for having, on the ZrO_2/CeO_2 matrix, both isolated Cu^{2+} ions and small copper clusters.

Quantification of H_2-TPR experiments was carried out and the values included in Table 1. It is clearly observed that the H_2 uptake increases until a CuO loading of 7 wt%. In every case it is observed an experimental H_2/Cu molar ratio always higher than that calculated for the total reduction of Cu, assuming that all the species are present as Cu^{2+}. This redundant hydrogen consumption in the H_2-TPR was found by various authors [17,53,55–57] and could be associated to spillover of hydrogen on the support surface that induces concurrent reduction of both copper oxide and ceria surface. In general it appears to be widely accepted in the literature that the addition of even small amounts of copper species to ceria strongly modifies the redox properties of both constituents of the catalytic system, compared to the pure materials. Ceria when interacting with transition metals can be reduced by H_2 even at temperatures lower than 200 °C [17,26,53,56,57].

When the influence of the zirconia amount is examined keeping copper amount constant, the H_2 consumed seems to depend on the nominal Zr/Ce molar ratio (Table 1, Fig. 3a). These data again underline that an intermediate ZrO_2 loading (7 wt%) maximize the amount of H_2 consumption.

3.6. XPS

Surface chemical information of fresh and used catalysts was obtained from XPS analysis. C 1s, O 2p, Cu 2p and Ce 3d core level spectra were recorded and decomposed to determine the species present on the catalyst surface. Short acquisition times were obliged to avoid, as much as possible, the photoreduction of Ce and Cu, especially in the case of Cu [43]. This gives rise to noisy Cu 2p core level spectra when the concentration of copper is low.

Table 3
Zr/Ce and Zr/Cu molar ratios, intensity shake up satellite/intensity main peak Cu $2p_{3/2}$ ratio and percentage of Ce^{3+}.

Sample		Zr/Ce	Zr/Cu	I_{sat}/I_{mp}	%Ce^{3+}
FCZCu27	Fresh	0.09	0.19	0.54	10.6
	Used	0.11	0.25	0.49	13.9
FCZCu37	Fresh	0.16	0.47	0.39	13.9
	Used	0.18	0.51	0.56	13.7
FCZCu57	Fresh	0.15	0.36	0.42	13.9
	Used	0.15	0.41	0.43	13.9
FCZCu77	Fresh	0.07	0.42	0.28	21.0
	Used	0.10	0.38	0.26	27.0
FCZCu107	Fresh	0.11	0.35	0.40	12.9
	Used	0.10	0.39	0.41	12.9
FCZCu73	Fresh	0.09	0.24	0.36	13.9
	Used	0.08	0.28	0.39	13.0
FCZCu75	Fresh	0.05	0.11	0.35	11.7
	Used	0.05	0.15	0.53	12.2

In all catalysts, C 1s core level spectra were decomposed into three contributions, the most important ones being that at 284.8 eV due to adventitious carbon, and that at 289.6–290.2 eV, assigned to the presence of surface carbonates. The presence of surface CO_3^{2-} is also observed on used samples after CO-PROX tests. The O 1s core level signals of the fresh and used catalysts always showed two contributions, one very intense at 529.2–529.4 eV assigned mainly to oxygen lattice of CeO_2; and other at 531.3–531.5 eV due to the presence of hydroxyls or carbonates at the surface of the samples, the amount ranging from 14–18 wt%.

The Cu 2p core level signals before and after catalysis are complex, due to the simultaneous presence of at least two different copper species. Fig. 4 shows the Cu 2p signal of fresh catalysts with the same nominal loading of copper and a different Zr/Ce ratio.

The presence of Cu $2p_{3/2}$ main peak centered at ca. 933 eV has been detected, although in some cases it is clearly observed the coexistence of two contribution at ca. 932.0 eV and 934.0 eV close to the binding energy reported for Cu^+ and CuO, respectively [20] suggesting the coexistence of both copper species even if its quantification cannot be done.

The presence of reduced copper species can be elucidated by considering the intensity of the satellite contribution at high binding energy together with the intensity of the main peak (I_{sat}/I_{mp}), this ratio being 0.55 if only CuO is present.

Data listed in Table 3 shows that all catalysts show a I_{sat}/I_{mp} value lower than that normally observed for CuO (0.55), indicating the presence of partially reduced copper species [51,58].

In the case of sample FCZCu27, the I_{sat}/I_{mp} value (0.54) is very close to that of for CuO. By increasing ZrO_2 content, this ratio reaches a value close to 0.4 for FCZCu37, FCZCu57 and FCZCu107. The exception being, FCZCu77, with the lowest I_{sat}/I_{mp} value (0.28) pointing to the presence of a larger amount of reduced copper species on this sample. After catalytic testing, the Cu 2p signal does not change (not shown) and the ratio I_{sat}/I_{mp} slightly changes, except for the sample FCZCu37 that presented a quite larger proportion of reduced Cu species.

Samples with different CuO loading showed I_{sat}/I_{mp} ratios ranging between 0.28 and 0.36. That is, even at low Cu loadings, the reduction degree attained for these samples (ZrO_2 loading 7 wt%) is better than for samples with a fixed amount of CuO and different ZrO_2 loadings.

Ce 3d core-level photoelectron spectrum is complex and can be decomposed in five spin–orbit doublets denoted as $v(n)$ and $u(n)$. Three doublets are ascribed to the presence of Ce^{4+}:

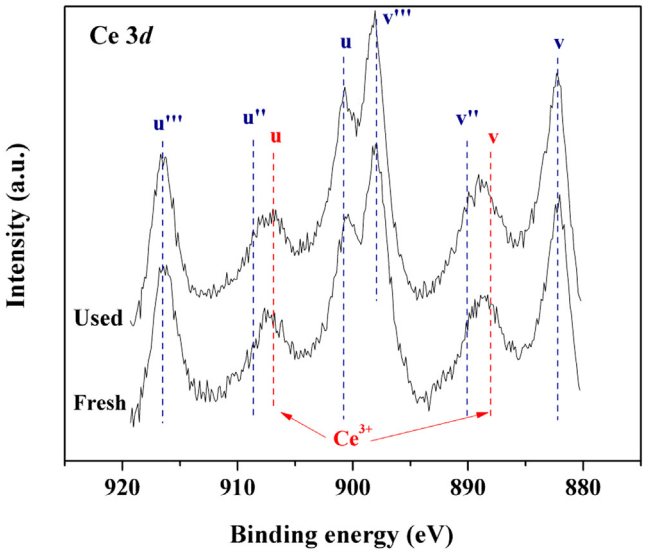

Fig. 5. Ce 3d core level spectra for FCZCu27 before and after catalytic test in CO-PROX.

v(~882.8 eV) and u(~901.3 eV)-Ce $3d^9$ $4f^2$ O $2p^4$; v''(~888.9 eV) and u''(~907.6 eV)-Ce $3d^9$ $4f^1$ O $2p^5$; v'''(~898.5 eV), u'''(~917.1 eV)-Ce $3d^9$ $4f^0$ O $2p^6$. Meanwhile two doublets: v_0(~881.2 eV) and u_0(~900 eV)-Ce $3d^9$ $4f^2$ O $2p^5$; v'(~885) and u'(~903.7 eV)-Ce $3d^9$ $4f^1$ O $2p^6$ are assigned to Ce^{3+} [31,42]. The reduction degree of cerium, expressed as % Ce^{3+}, was calculated by taking into account these ten contributions. Fig. 5 shows the Ce 3d core level spectra of FCZCu27 sample before and after one cycle of catalytic activity, as an example. In general, the main oxidation state of Ce is Ce^{4+} with all the components (blue lines) clearly visible, while the component v_0(~881 eV) of Ce^{3+} is hardly noticeable for these samples. The spectra before and after catalysis are barely modified indicating that ceria-based support seems very stable.

An estimation of the percentages of reduced cerium ions (Ce^{3+}) for the studied samples is compiled in Table 3. The obtained values are more or less the same for all the samples ranging from 10.6 and 14.0, the exception is FCZCu77 sample, in which the Ce reduction degree appears to be much higher (21%). Moreover, after catalytic testing only FCZCu77 sample displays an important increase in the percentage of %Ce^{3+}, from 21 to 27%.

The surface atomic composition (Table 3) shows that Zr/Ce surface ratio was higher than the bulk one determined from ICP-OES analysis for FCZCu27, FCZCu37, and FCZCu57, indicating than Zr species are mainly located on the surface. Instead, for samples with a higher ZrO_2 content, FCZCu77 and FCZCu107, these values are lower than the bulk ones. FCZCu77 showed the lowest Zr/Ce ratio, that is a cerium enriched surface. Considering samples with different CuO contents, the obtained values are lower than the bulk one (0.11).

Finally, the surface Zr/Cu ratio sharply increased from FCZCu27 (0.19) to FCZCu37 (0.47) sample, further ZrO_2 additions do not produce an increase of the Zr/Cu ratios calculated by XPS, even a slight decrease is observed (see Table 3). Considering the Zr/Cu ratio for samples with different CuO content, the FCZCu77 presented the highest value, suggesting that, in spite of presenting the higher amount of copper, they are homogeneously distributed and not concentrated on the catalyst surface.

3.7. CO preferential oxidation activity

The catalytic activity of the samples was evaluated in the CO-PROX reaction. The experiments were carried out in the 40–190 °C temperature range by using a synthetic reformate gas (1.25% CO, 1.25% O_2, and 50.0% H_2, He balance). The carbon balance showed that, in all the catalytic tests, the CO_2 production was in good agreement with the CO consumption, ruling out coking occurrence. Both methanation and reverse water gas shift reaction (RWGS) were found negligible below 200 °C in our experimental conditions.

All samples were tested twice. The second catalytic cycle was carried out using the same conditions used in the first one, after heating in air flow in situ at 400 °C for 1 h. The second reaction profile was in all cases identical to the first one.

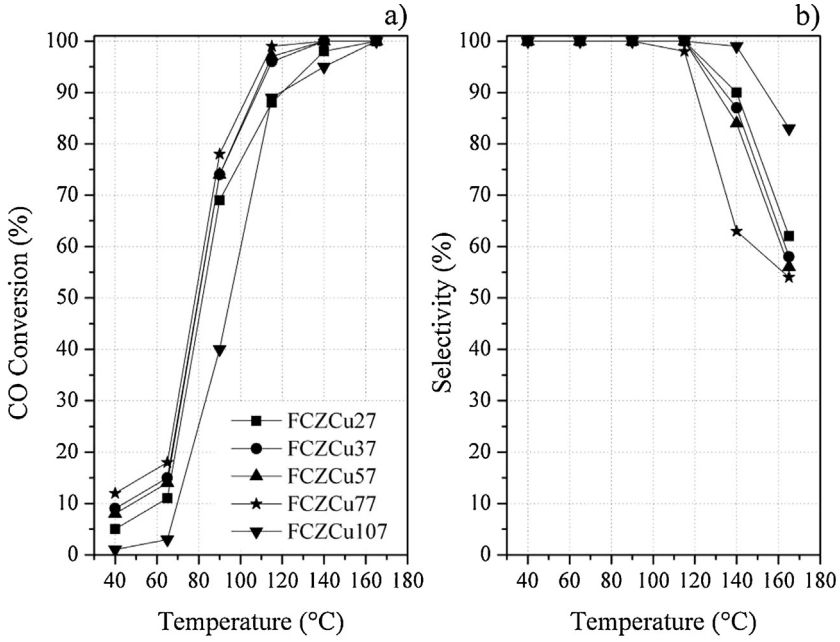

Fig. 6. Samples with a fixed content of copper and variable loadings of zirconium. Dependencies of: (a) CO conversion (%) and (b) selectivity to CO_2 (%) as a function of temperature. Operating conditions: GHSV = 22000 h^{-1}; λ = 2; 1.25% CO, 1.25% O_2, and 50% H_2, He balance (vol%).

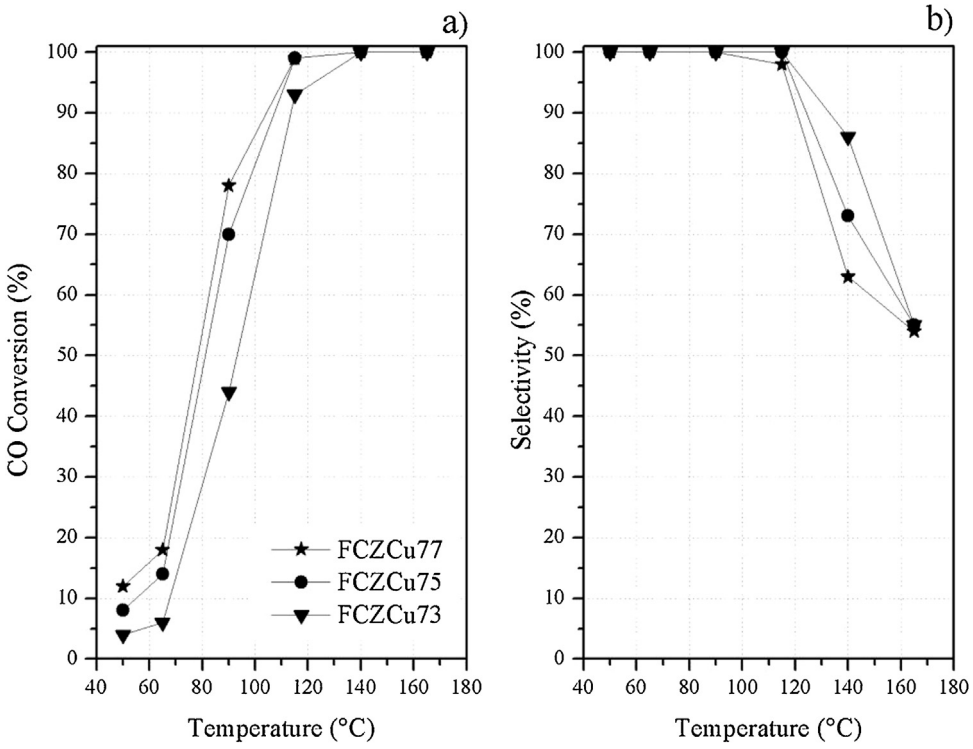

Fig. 7. Samples with a fixed content of zirconium and variable loadings of copper. Dependencies of: (a) CO conversion (%) and (b) selectivity to CO_2 (%) as a function of temperature. Operating conditions: GHSV = 22000 h^{-1}; λ = 2; 1.25% CO, 1.25% O_2, and 50% H_2, He balance (vol%).

Table 4
Apparent activation energies and T_{50} values in the CO-PROX for the catalysts FCZCu*xy*.

Sample	$E_{a\ standardfeed}$ (kJ mol^{-1})	$T_{50\ standardfeed}$ (°C)
FCZCu27	44 ± 2	82
FCZCu37	37 ± 2	80
FCZCu57	35 ± 2	80
FCZCu77	31 ± 2	78
FCZCu107	65 ± 3	95
FCZCu73	46 ± 2	93
FCZCu75	37 ± 2	81

3.7.1. *Effect of the zirconia to ceria molar ratio at the same CuO loading*

In a first set of measurements, the catalysts containing different ZrO_2/CeO_2 molar ratio and the same amount of copper oxide were compared (Fig. 6).

The CO conversion, for this set of catalytic runs, increased with the temperature and reached 100% at 140 °C for FCZCu37, FCZCu57, and FCZCu77 catalysts and above 160 °C for FCZCu27 and FCZCu107 (Fig. 6a). The selectivity to CO_2 (Fig. 6b) was about 100%, for all the catalysts, till 115 °C and decreased, above this temperature, for the more active ones in the CO conversion reaction. It should be noted that, considering the reaction stoichiometry, the oxygen excess factor used and the CO conversion values, the O_2 consumption is exclusively attributable to oxidation of CO–CO_2. The different nominal Zr/Ce molar ratio appears to have a significant influence on the catalytic performance of the Ce–Zr–Cu oxide system and samples with identical nominal copper loading (with about 7.0 wt% CuO), exhibit a quite different catalytic behavior.

The FCZCu77 catalyst exhibited much higher catalytic activity than the others samples: it was able to oxidize CO in the interval 115–160 °C, achieving a conversion >98% with maximum selectivity of 98% in this temperature range. In Table 4, the interpolated T_{50} values are reported (temperature at which 50% of CO conversion is reached). The T_{50} temperature was 78 °C for FCZCu77 and it slightly increased for the samples with a lower zirconia content. On the contrary, the difference is significant for the sample with a higher Zr content, FCZCu107, with a T_{50} higher of about 17 °C (Fig. 6a). These catalytic results showed that an optimum Zr/Ce molar ratio is required for the best catalytic performance over the studied nanostructured Ce/Zr/Cu oxide systems with a flower-like morphology.

3.7.2. *Effect of the copper oxide loading at the same zirconia to ceria molar ratio*

The activity of FCZCu*xy* catalysts for the catalytic activity in the CO-PROX can also be affected by the content of copper in the catalyst. A second set of measurements was made to evaluate the effect of the copper oxide. For this test it was considered the catalyst containing the better-performing amount of zirconium oxide, selected among the catalysts with different zirconia to ceria molar ratio, that is FCZCu77. The CuO content was now lowered from 7 to 5 and 3 wt%. (samples FCZCu77, FCZCu75, and FCZCu73 respectively). The corresponding catalytic results are represented in Fig. 7. At the lowest tested temperature the CO conversion (Fig. 7a) was 4, 8, and 12% going from the lower amount of copper oxide to the higher one, increases with the temperature, reaching 100% of conversion at 140 °C for all the catalysts. At 115 °C both FCZCu77 and FCZCu75 catalysts reached more than 98% of CO conversion. The FCZCu73 catalyst showed lower catalytic performances reaching at 115 °C less than 94% of CO conversion. The selectivity to CO_2 (Fig. 7b) is 100% until 115 °C, for all the catalysts, and decreased, above this temperature, for the more active ones in the CO conversion reaction.

Apparent activation energies E_a, calculated from Arrhenius plot, for the reaction of preferential CO oxidation were calculated and included in Table 4 jointly with the interpolated T_{50}. These E_a values are in good agreement with those reported in literature for the CO-PROX process over CuO/CeO_2 catalysts, that were found in

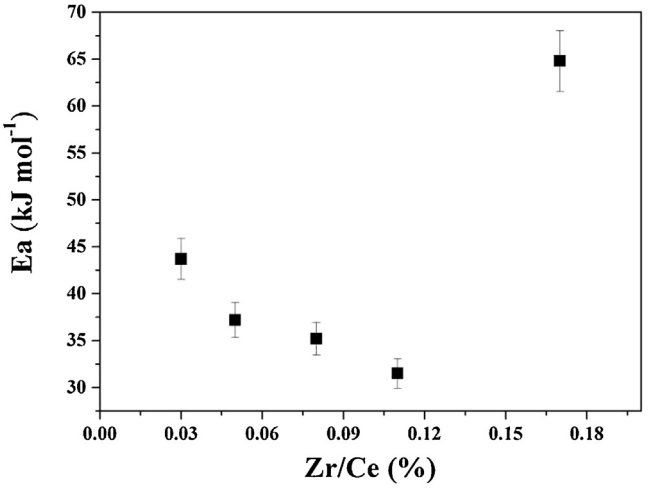

Fig. 8. Apparent activation energies versus Zr/Ce atomic ratio for FCZCu*x*7 catalysts.

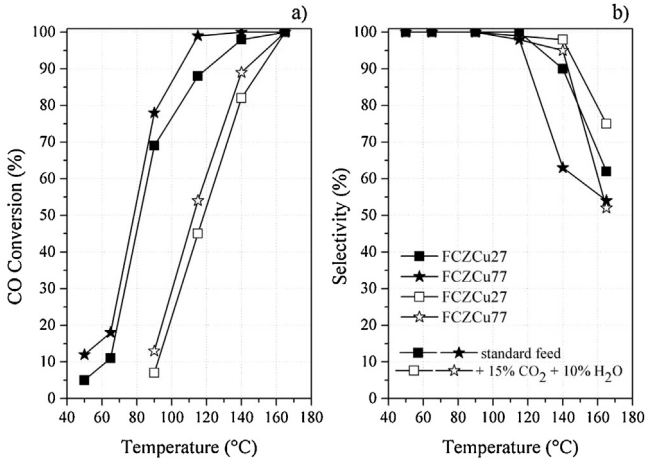

Fig. 9. Comparison of samples with a fixed content of copper oxide (7 wt%) and variable loadings of zirconium oxide. Dependencies of: (a) CO conversion and (b) selectivity toward CO_2 over the title catalysts, before and after the addition to the standard feed of 15 vol% of CO_2 and 10 vol% H_2O. Operating conditions: GHSV = 22,000 h^{-1}; $\lambda = 2$; 1.25% CO, 1.25% O_2, 50% H_2, 15% CO_2, and 10% H_2O, He balance (vol%).

the range 40–60 kJ mol^{-1} [59,60]. Other authors [61] reported for $CuO/Ce_{1-x}Cu_xO_{2-\delta}$ and $Ce_{1-x}Cu_xO_{2-\delta}$ catalysts, apparent activation energy values of 42 ± 2 kJ mol^{-1} and 95 ± 5 kJ mol^{-1} respectively.

Among the CuO–CeO_2–ZrO_2 nanostructured catalysts studied, the apparent activation energy E_a seems to depend, for the same amount of CuO, on the zirconia to ceria molar ratio (Fig. 8). The FCZCu77 catalyst, containing 7 wt% of copper oxide, shows an $E_a = 31 \pm 2$ kJ mol^{-1} which is the lowest value found among the catalyst studied, indicating that the presence of an intermediate amount of nominal zirconia ($ZrO_2/CeO_2 = 0.11$), in our reaction conditions, significantly lowers the activation energy of preferential CO oxidation. Beside, FCZCu57 and FCZCu37 catalysts show an activation energy value not far from that of FCZCu77. When only a slightly lower ($ZrO_2/CeO_2 = 0.03$) or a slightly higher ($ZrO_2/CeO_2 = 0.17$) zirconia to ceria molar ratio was used, E_a was found to increase (Fig. 8). CuO amount also play an important role observing, in fact, in the studied samples, a sharp decrease in E_a by increasing the mol of CuO loaded.

Catalytic results show that the catalyst composition seems to determine crystalline phases in the sample, their reducibility and the dispersion of active species. From XRD results, FCZCu77 sample showed the highest amount of undetectable very small CuO nanoparticles (4.6 wt%), also evidenced from H_2-TPR data that display an α-peak more pronounced attesting the presence of a higher amount of very small copper oxide species in intimate contact with ceria.

Finally, a durability test was performed on the sample with the best catalytic performances, FCZCu77 (not shown). The reaction was monitored for 150 h maintaining the temperature constant at 115 °C, using GHSV = 22,000 h^{-1}; $\lambda = 2$; 1.25% CO, 1.25% O_2, and 50% H_2, He balance (vol%). The catalyst showed a diminution of CO conversion from 99% to 94% within the first 6 h, remaining stable for the further operation time.

The effect of the presence of CO_2 and H_2O in the feed on the activity and the selectivity was also examined, since these species are present in significant amount in the reformate gas and are also the reaction products. In order to check the effect of a CO_2 and H_2O in the standard feed on catalyst activity, 15% CO_2 and 10% H_2O (vol%) were simultaneously added to the feed stream (Fig. 9) on the most active catalyst, FCZCu77, and on the catalyst with the lower zirconia content, FCZCu27, for comparison. The addition of CO_2 and H_2O to the feed considerably decreased the catalytic activity and increased the reaction temperature of about 30–40 °C to get the same CO conversion observed in the absence of CO_2 and H_2O (Fig. 9a) The selectivity to CO_2 for FCZCu27 and FCZCu77 (Fig. 9b), when CO conversion reaches 100%, drops down 75 and 52%, respectively.

The negative effect of H_2O can be ascribed to the blockage of the active sites by the water adsorbed and the inhibiting effect of adding CO_2 in the stream can be due to the competitive adsorption between CO_2 and CO on the catalyst surface and the formation of carbonates. The inhibiting effect of the presence of CO_2 (15 vol%) in the reaction mixture of CO-PROX reaction on the performance of CuO/CeO_2 catalysts has been deeply investigated by Di Benedetto et al. [62]. They suggest that CO_2 depresses CO oxidation up to 160 °C, its effect being negligible at higher temperatures. Two sites on CeO_2 support have been identified by a mathematical model: one modified by the strong interaction between Ce and Cu when copper is added and an additional site associated to less interacting copper for CuO/CeO_2 catalysts. Although ceria gives a large contribution to CO_2 adsorption, the sites present in larger amount rapidly desorb CO_2 in the typical temperature range of CO-PROX reaction (80–150 °C), especially when copper modification induces a decrease of desorption activation energy, thus suggesting that these centres are involved in CO oxidation.

No many studies are reported in literature on CuO–CeO_2–ZrO_2 systems active in the CO-PROX reaction. Among them, the effect of Zr and La ions on the properties of CuO–CeO_2 catalyst was recently reported [63], showing that low amounts of Zr increase the catalytic activity, by increasing the interaction between cerium and copper and then increasing the interface where the reaction of preferential oxidation occurs. The catalytic performance of the CuO–CeO_2–ZrO_2 flower-like catalysts here described can be considered very good in comparison with other Cu–Ce–Zr based systems and, as for other Cu-based catalysts for CO-PROX reaction, it has been found that a strong interaction between the active copper species and the reducible support is a prerequisite for a high activity in the selective CO oxidation. Realizing the importance of the preparation method that can provide a large amount of active sites for CO oxidation, other particular Cu-based systems have been described in literature. A CuO–CeO_2 catalyst was prepared by hydrothermal synthesis in the presence of surfactant CTABr [64] or Cu-based systems supported on reducible oxide/hydroxide different from ceria [65] and an inverse CeO_2/CuO catalyst [66], all of them showing that the strong interaction between the components is responsible for the high activity in the selective CO oxidation at low temperatures.

4. Conclusions

The role of the chemical composition for samples containing $CuO–ZrO_2–CeO_2$, prepared by a simple and low-cost synthetic strategy was studied for the CO-PROX reaction. It was observed that the physico-chemical properties and catalytic performance of flower-like $CuO–ZrO_2–CeO_2$ systems, with a relatively low amount of zirconia, are highly dependent on the Zr/Ce atomic ratio and CuO loaded. The different Zr/Ce atomic ratios appear to have a significant influence on the catalytic performance of the Ce–Zr–Cu oxide system and samples with the same copper loading (with about 7.0 wt% CuO), exhibit a quite different catalytic behavior. Sample FCZCu77, with a nominal atomic ratio Zr/Ce = 0.11 and with 7 wt% of copper oxide, shows very good catalytic performances. XRD analysis showed that this catalyst presents the higher fraction of undetectable CuO (4.6 wt%). It indicates that the CeO_2 doped with an optimal amount of zirconium through a slowly co-precipitation method can form a material with improved CuO dispersion and interaction with CeO_2. H_2-TPR data confirmed that FCZCu77 sample exhibited small finely dispersed CuO particles and interacting with ceria. The formation of highly dispersed Cu species could be ascribed to the known disorder and defects induced by the presence of zirconia in quite small quantities in the ceria lattice.

Activity towards CO oxidation in hydrogen rich streams was correlated with Zr/Ce molar ratio, CuO content and the reducibility of copper species. The most active catalyst, FCZCu77, containing only 7 wt% of zirconia exhibited much higher catalytic activity than the others samples, achieving a CO conversion close to 100% with maximum selectivity of 98% in the range 115–160 °C, the operation window becoming broader as Zr content in the support both increases and decreases.

Acknowledgements

Ca' Foscari University of Venice, Consortium INSTM, the National Spanish Project CTQ2012-37925-C03-03 and FEDER fundsand Junta de Andalucía Project P12-RNM-1565 are acknowledged for financial support.

References

[1] D. Deng, J. Jesus, H. Saltsburg, M. Flytzani-Stephanopoulos, Appl. Catal. A: Gen. 291 (2005) 126–135.
[2] G. Avgouropoulos, M. Manzoli, F. Boccuzzi, T. Tabakova, J. Papavasiliou, T. Ioannides, V. Idakiev, J. Catal. 256 (2008) 237–247.
[3] L. Ilieva, G. Pantaleo, I. Ivanov, A. Maximova, R. Zanella, Z. Kaszkur, A.M. Venezia, D. Andreeva, Catal. Today 158 (2010) 44–55.
[4] G.Q. Yi, H.W. Yang, B.D. Li, H.Q. Lin, K. Tanaka, Y.Z. Yuan, Catal. Today 157 (2010) 83–88.
[5] T. Tabakova, G. Avgouropoulos, J. Papavasiliou, M. Manzoli, F. Boccuzzi, K. Tenchev, F. Vindigni, T. Ioannides, Appl. Catal. B: Environ. 101 (2011) 256–265.
[6] O. Pozdnyakova, D. Teschner, A. Wootsch, J. Krohnert, B. Steinhauer, H. Sauer, L. Toth, F.C. Jentoft, A. Knop-Gericke, Z. Paal, R. Schlogl, J. Catal. 237 (2006) 1–16.
[7] N. Bion, F. Epron, M. Moreno, F. Marino, D. Duprez, Top. Catal. 51 (2008) 76–88.
[8] S.J. Huang, K. Hara, A. Fukuoka, Energy Environ. Sci. 2 (2009) 1060–1068.
[9] O. Pozdnyakova, D. Teschner, A. Wootsch, J. Krohnert, B. Steinhauer, H. Sauer, L. Toth, F.C. Jentoft, A. Knop-Gericke, Z. Paal, R. Schlogl, J. Catal. 237 (2006) 17–28.
[10] A.I. Boronin, E.M. Slavinskaya, I.G. Danilova, R.V. Gulyaev, Y.I. Amosov, P.A. Kumetsov, I.A. Polukhina, S.V. Koscheev, V.I. Zaikovskii, A.S. Noskov, Catal. Today 144 (2009) 201–211.
[11] Y.Q. Huang, A.Q. Wang, L. Li, X.D. Wang, D.S. Su, T. Zhang, J. Catal. 255 (2008) 144–152.
[12] A. Martinez-Arias, A.B. Hungria, M. Fernandez-Garcia, J.C. Conesa, G. Munuera, J. Power Sources 151 (2005) 32–42.
[13] D. Gamarra, C. Belver, M. Fernandez-Garcia, A. Martinez-Arias, J. Am. Chem. Soc. 129 (2007) 12064–12065.
[14] D. Gamarra, G. Munuera, A.B. Hungria, M. Fernandez-Garcia, J.C. Conesa, P.A. Midgley, X.Q. Wang, J.C. Hanson, J.A. Rodriguez, A. Martinez-Arias, J. Phys. Chem. C 111 (2007) 11026–11038.
[15] A. Gómez-Cortés, Y. Márquez, J. Arenas-Alatorre, G. Díaz, Catal. Today 133 (2008) 743–749.
[16] H.C. Lee, D.H. Kim, Catal. Today 132 (2008) 109–116.
[17] T. Caputo, L. Lisi, R. Pirone, G. Russo, Appl. Catal. A: Gen. 348 (2008) 42–53.
[18] F. Marino, B. Schonbrod, M. Moreno, M. Jobbagy, G. Baronetti, M. Laborde, Catal. Today 133 (2008) 735–742.
[19] D. Gamarra, M. Fernandez-Garcia, C. Belver, A. Martinez-Arias, J. Phys. Chem. C 114 (2010) 18576–18582.
[20] E. Moretti, L. Storaro, A. Talon, M. Lenarda, P. Riello, R. Frattini, M.D.M. de Yuso, A. Jimenez-Lopez, E. Rodriguez-Castellon, F. Ternero, A. Caballero, J.P. Holgado, Appl. Catal. B: Environ. 102 (2011) 627–637.
[21] A. Martínez-Arias, R. Cataluna, J. Conesa, J. Soria, J. Phys. Chem. B 102 (1998) 809–817.
[22] G.R. Kosmambetova, V.I. Gritsenko, P.E. Strizhak, A.M. Korduban, Theor. Exp. Chem. 42 (2006) 133–138.
[23] K. Sirichaiprasert, A. Luengnaruemitchai, S. Pongstabodee, J. Hydrogen Energy 32 (2007) 915–926.
[24] A. Martinez-Arias, M. Fernandez-Garcia, O. Galvez, J.M. Coronado, J.A. Anderson, J.C. Conesa, J. Soria, G. Munuera, J. Catal. 195 (2000) 207–216.
[25] S.P. Wang, T.Y. Zhang, Y. Su, S.R. Wang, S.-M. Zhang, B.L. Zhu, S.H. Wu, Catal. Lett. 121 (2008) 70–76.
[26] L. Kundakovic, M. Flytzani-Stephanopoulos, Appl. Catal. A: Gen. 171 (1998) 13–29.
[27] G. Avgouropoulos, T. Ioannides, H. Matralis, Appl. Catal. B: Environ. 56 (2005) 87–93.
[28] A. Martínez-Arias, A.B. Hungría, G. Munuera, D. Gamarra, Appl. Catal. B: Environ. 65 (2006) 207–216.
[29] T. Caputo, R. Pirone, G. Russo, Kinet. Catal. 47 (2006) 761–764.
[30] E. Moretti, L. Storaro, A. Talon, M. Lenarda, Catal. Commun. 10 (2009) 522–527.
[31] E. Moretti, M. Lenarda, P. Riello, L. Storaro, A. Talon, R. Frattini, A. Reyes-Carmona, A. Jiménez-López, E. Rodríguez-Castellón, Appl. Catal. B: Environ. 129 (2013) 556–565.
[32] P. Fornasiero, G. Balducci, R. Di Monte, J. Kăspar, V. Sergo, G. Gubitosa, A. Ferrero, M. Graziani, J. Catal. 164 (1996) 173–183.
[33] A. Martinez-Arias, M. Fernández-Garcia, O. Gálvez, J.-M. Coronado, J.A. Anderson, J.C. Conesa, J. Soria, G. Munera, J. Catal. 195 (2000) 207–216.
[34] J.L. Cao, Q.F. Deng, J. Mater. Sci. 44 (2009) 6663–6669.
[35] M.P. Yeste, J.C. Hernández, S. Trasobares, S. Bernal, G. Blanco, J.J. Calvino, J.A. Pérez-Omil, J.M. Pintado, Chem. Mater. 20 (2008) 5107–5113.
[36] Y. Nagai, T. Yamamoto, T. Tanaka, S. Yoshida, T. Nonaka, T. Okamoto, A. Suda, M. Sugiura, Top. Catal. 47 (2008) 137–147.
[37] I. Atribak, N. Guillén-Hurtado, A. Bueno-López, A. García- García, Appl. Surf. Sci. 256 (2010) 7706–7712.
[38] S. Abdollahzdeh-Ghom, C. Zamani, T. Andreu, M. Epifani, J.R. Morante, App. Catal. B: Environ. 108–109 (2011) 32–38.
[39] P. Ratnasamy, D. Srinivas, C.V.V. Satyanarayana, P. Manikandan, R.S. Senthil Kumaran, M. Sachin, V.N. Shetti, J. Catal. 221 (2004) 455–461.
[40] M. Manzoli, R. Di Monte, F. Boccuzzi, S. Coluccia, J. Kăspar, Appl. Catal. B 61 (2005) 192–205.
[41] X.F. Dong, H.B. Zou, W.-M. Lin, Int. J. Hydrogen Energy 31 (2006) 2337–2344.
[42] E. Moretti, L. Storaro, A. Talon, R. Moreno-Tost, E. Rodríguez-Castellón, A. Jiménez-López, M. Lenarda, Catal. Lett. 129 (2009) 323–330.
[43] J. Zhu, L. Zhang, Y. Deng, B. Liu, L. Dong, F. Gao, K. Sun, L. Dong, Y. Chen, Appl. Catal. B: Environ. 96 (2010) 449–457.
[44] Á. Reyes-Carmona, A. Arango-Díaz, E. Moretti, A. Talon, L. Storaro, M. Lenarda, A. Jiménez-López, E. Rodríguez-Castellón, J. Power Sources 196 (2011) 4382–4387.
[45] S. Poulston, P.M. Parlett, P. Stone, M. Bowker, Surf. Interface Anal. 24 (1996) 811–820.
[46] G. Avgouropoulos, T. Ioannides, Appl. Catal. A: Gen. 244 (2003) 155–167.
[47] P. Bera, K.R. Priolkar, P.R. Sarode, M.S. Hegde, S. Emura, R. Kumashiro, N.P. Lalla, Chem. Mater. 14 (2002) 3591–3601.
[48] M.-F. Luo, Y.-J. Zhong, X.-X. Yuan, X.-M. Zheng, Appl. Catal. A: Gen. 162 (1997) 121–131.
[49] J. Xiaoyuan, L. Guanglie, Z. Renxian, M. Jianxin, C. Yu, Z. Xiaoming, Appl. Surf. Sci. 173 (2001) 208–220.
[50] L. Qiu, F. Liu, L. Zhao, Y. Ma, J. Yao, Appl. Surf. Sci. 252 (2006) 4931–4935.
[51] G. Avgouropoulos, T. Ioannides, Appl. Catal. B: Environ. 67 (2006) 1–11.
[52] H. Zou, X. Dong, W. Lin, Appl. Surf. Sci. 253 (2006) 2893–2898.
[53] A. Pintar, J. Batista, S. Hočevar, J. Colloid Interface Sci. 285 (2005) 218–231.
[54] S. Piras, A. Colussi, A. Trovarelli, V. Sergo, J. Llorca, R. Psaro, L. Sordelli, J. Phys. Chem. B 109 (2005) 11110–11118.
[55] P. Zimmer, A. Tschöpe, R. Birringer, J. Catal. 205 (2002) 339–345.
[56] R. Pérez-Hernándes, A. Gutiérrez-Martínez, C.E. Gutiérrez-Wing, Int. J. Hydrogen Energy 32 (2007) 2888–2894.
[57] X. Tang, B. Zhang, Y. Li, Y. Xu, Q. Xin, W. Shen, Catal. Today 93–95 (2004) 191–198.
[58] H.X. Mai, L.D. Sun, Y.W. Zhang, R. Si, W. Feng, H.P. Zhang, H.C. Liu, C.H. Yan, J. Phys. Chem. B 109 (2005) 24380–24385.
[59] G. Sedmak, S. Hočevar, J. Levec, J. Catal. 213 (2003) 135–150.
[60] M. Moreno, G.T. Baronetti, M.A. Laborde, F.J. Marino, Int. J. Hydrogen Energy 33 (2008) 3538–3542.
[61] A.-P. Jia, G.-S. Hu, L. Meng, Y.-L. Xie, J.-Q. Lu, M.-F. Luo, J. Catal. 289 (2012) 199–209.

[62] A. Di Benedetto, G. Landi, L. Lisi, G. Russo, Appl. Catal. B: Environ. 142–143 (2013) 169–177.
[63] J.S. Moura, J. da Silva Lima Fonseca, N. Bion, F. Epron, T. de Freitas Silva, C. Guimarães Maciel, J. Mansur Assaf, M. do Carmo Rangel, Catal. Today 228 (2014) 40–50.
[64] M. Tada, R. Bal, X. Mu, R. Coquet, S. Namba, Y. Iwasawa, Chem. Commun. 44 (2007) 4689–4691.
[65] B. Qiao, A. Wang, J. Lin, L. Li, D. Su, T. Zhang, Appl. Catal. B 105 (2011) 103–109.
[66] A. Hornés, A.B. Hungría, P. Bera, A. López Cámara, M. Fernández-García, A. Martínez-Arias, L. Barrio, M. Estrella, G. Zhou, J.J. Fonseca, J.C. Hanson, J.A. Rodriguez, J. Am. Chem. Soc. 132 (2010) 34–35.